

Electronic properties of the three-band Hubbard model

M. B. Zöfl, Th. Maier, Th. Pruschke, J. Keller

Institut für Theoretische Physik I, Universität Regensburg, Universitätsstr. 31, 93053 Regensburg, Germany

Received: date / Revised version: date

Abstract. We study the electronic band-structure and transport properties of a CuO_2 -plane within the three-band Hubbard model. The Dynamical Mean-Field Theory (DMFT) is used to solve the many particle problem. The calculations show that the optical gap Δ_{opt} is given by excitations from the lower Hubbard band into the so called Zhang-Rice singlet band. The optical gap Δ_{opt} turns out to be considerably smaller than the charge transfer energy Δ ($\Delta = \epsilon_p - \epsilon_d$) for a typical set of parameters, which is in agreement with experiment. For the two-dimensional CuO_2 -plane we investigated the dependency of the shape of the Fermi surface on the different hopping parameters t_{CuO} and t_{OO} . A value $t_{\text{OO}}/t_{\text{CuO}} > 0$ leads to a Fermi surface surrounding the M point. An additional different static shift of the oxygen energies is also considered to calculate the electronic response due to a displacement of the oxygen atoms given by a frozen phonon. The density-density correlation for the oxygen orbitals is linear in doping for both hole and electron doping but shows a different temperature dependency in the two regimes. In the first case it is temperature independent and increases upon doping, which leads to an increasing electron-phonon coupling for the B_{1g} -mode in high- T_c superconductors.

PACS. 71.27.+a Strongly correlated electron systems – 71.30.+h Metal-insulator transitions and other electronic transitions – 74.25.Fy Transport properties (electric conductivity) – 74.25.Jb Electronic structure – 74.25.Kc Phonons

1 Introduction

Since the discovery of high temperature superconductivity by Bednorz and Müller [1] it is a challenging problem to find a theoretical description of this phenomenon. However, even in the normal state the electronic structure of the new compounds, which show superconductivity, is extremely hard to describe due to electronic correlations. A characteristic feature of the high- T_c compounds is a unit cell with one or more CuO_2 -planes, which are responsible for the superconductivity [2]. The most simple description of such a CuO_2 -plane is achieved within the one-band Hubbard model [3], which considers one effective 3d orbital of Cu in a tight-binding model in the presence of a local Coulomb repulsion U_d . This model describes well the properties of an insulator, because it reproduces the so called Mott-Hubbard metal-insulator transition [4]. However, this simple model leads to a wrong description of the planes concerning the doping dependency of various properties, such as the asymmetric magnetic doping-temperature phase diagram [5].

The oxygen atoms in the CuO_2 -plane, respectively the $2p$ -orbitals of these atoms introduce a further degree of freedom and the strongest hybridization takes place between the $\text{Cu-}3d_{x^2-y^2}$ orbital and the $\text{O-}2p_{x/y}$ orbitals [6]. Therefore they form the lowest lying bonding state and the

highest lying anti-bonding state. Choosing the most simple description of the CuO_2 -plane one is led to the hole picture and one has to consider the latter state, which is occupied with one hole. In order to describe the additional degrees of freedom, one has to solve at least a so called three-band Hubbard model or Emery model [7], with two additional oxygen orbitals $2p_x$ and $2p_y$, which are included in a tight-binding manner. For the sake of simplicity all Coulomb energies but U_d are neglected. Within this model one is able to describe a doped charge transfer insulator, which gives a more realistic picture of the planes in a high- T_c compound. The three-band model has recently been studied by Schmalian et al. [8] using a generalized dynamical mean-field (DMFT) approach and our contribution is based on their approach. Watanabe et al. [9] discussed the metal-insulator transition in a two-band Hubbard model in infinite dimensions and discovered the coexistence of metallic and antiferromagnetic phases. This was also found by Maier et al. [10], who additionally reported about an asymmetric magnetic doping-temperature phase diagram within our approach, which shows, that the antiferromagnetic phase is more stable upon electron doping than upon hole doping.

In this paper the DMFT approach of Schmalian et al. [8] for the three-band Hubbard model is used. Several extra features in two spatial dimensions were added, such as an oxygen-oxygen hopping process and a splitting of the oxygen energy levels. We discuss results for the one-

particle spectra of the orbitals and for the in-plane conductivity for hole and electron doped systems considering a semi-elliptic density of states. We further discuss, for the case of a two dimensional system, how an additional oxygen-oxygen hopping process affects the shape of the Fermi surface. Finally a static shift of the oxygen energies due to a displacement given by a frozen phonon is considered in order to calculate the static density-density correlation, which describes the electronic response to this kind of distortion. A summary will conclude the paper.

2 The three-band Hubbard model

The starting point of our approach is a simplified Emery Hamiltonian [7] describing the dynamics of holes in a doped CuO₂-plane. The nearest neighbour hopping processes between the 3d-orbital of the Cu-atom and the 2p_x-/ 2p_y-orbital of the O-atom ($t_{i,j\nu}$ and $t'_{i\kappa,j\nu}$) are taken into account. ε_d , ε_{p_x} and ε_{p_y} represent the energy levels of each orbital and μ the chemical potential, in addition a local Coulomb energy U_d for the case of a doubly occupied d-orbital, which is responsible for the correlations.

$$\begin{aligned} \hat{H} = & \sum_{i,\sigma} (\varepsilon_d - \mu) d_{i,\sigma}^\dagger d_{i,\sigma} + \sum_{i,\nu,\sigma} (\varepsilon_{p_\nu} - \mu) p_{i\nu,\sigma}^\dagger p_{i\nu,\sigma} \\ & + \sum_{i,j,\nu,\sigma} (t_{i,j\nu} d_{i,\sigma}^\dagger p_{j\nu,\sigma} + h.c.) + \sum_{\substack{i,\nu,j,\kappa,\sigma \\ i \neq j, \nu \neq \kappa}} t'_{i\kappa,j\nu} p_{i\kappa,\sigma}^\dagger p_{j\nu,\sigma} \\ & + \sum_i U_d d_{i,\uparrow}^\dagger d_{i,\uparrow} d_{i,\downarrow}^\dagger d_{i,\downarrow}. \end{aligned} \quad (1)$$

As mentioned earlier, this Hamiltonian is able to describe a doped charge transfer insulator, which is characterized by the charge transfer energy $\Delta = \varepsilon_p - \varepsilon_d$. The relation $U > \Delta$ ensures the system of being in the charge transfer regime [11]. This relation typically holds for parameters obtained from a first principles calculation (see table 1). The gauge invariance of the Hamiltonian allows us to

Table 1. Parameters for a three-band model (in eV) calculated with a constrained first principles calculation for La₂CuO₄ done by Hybertsen et al. [12].

Δ	t	t'	U_d	U_p	U_{pd}	U_{pp}
3.6	1.3	0.65	10.5	4	1.2	0

choose the phase of the wave functions freely. We use the phase convention shown in figure 1, which determines all phases of the considered hopping processes. The transformation into \mathbf{k} -space leads us to the following Hamiltonian (for simplicity we show the non-interacting part only):

$$H_o = \sum_{\mathbf{k},\sigma} (d_{\mathbf{k}\sigma}^\dagger, p_{x\mathbf{k}\sigma}^\dagger, p_{y\mathbf{k}\sigma}^\dagger) \underline{h}(\mathbf{k}) \begin{pmatrix} d_{\mathbf{k}\sigma} \\ p_{x\mathbf{k}\sigma} \\ p_{y\mathbf{k}\sigma} \end{pmatrix}, \quad (2)$$

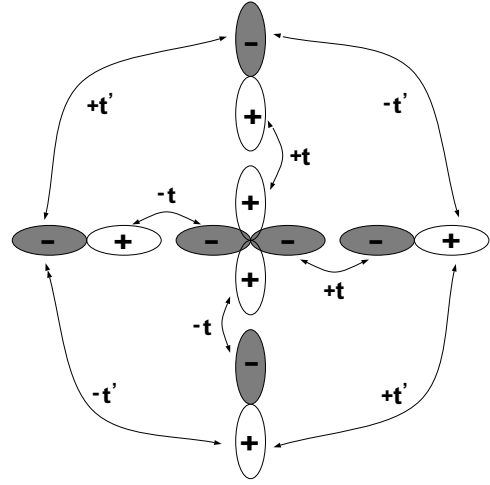


Fig. 1. Used phase convention, which determines the phases of all hopping processes.

with the matrix $\underline{h}(\mathbf{k})$:

$$\underline{h}(\mathbf{k}) = \begin{pmatrix} \varepsilon_d - \mu & 2it \sin(\mathbf{k}\mathbf{x}) & 2it \sin(\mathbf{k}\mathbf{y}) \\ -2it \sin(\mathbf{k}\mathbf{x}) & \varepsilon_{p_x} - \mu & -4t' \sin(\mathbf{k}\mathbf{x}) \sin(\mathbf{k}\mathbf{y}) \\ -2it \sin(\mathbf{k}\mathbf{y}) & -4t' \sin(\mathbf{k}\mathbf{x}) \sin(\mathbf{k}\mathbf{y}) & \varepsilon_{p_y} - \mu \end{pmatrix}. \quad (3)$$

This uncorrelated Hamiltonian can be diagonalized easily. In order to treat the strong Coulomb repulsion U_d , we use the dynamical mean-field theory, where the lattice problem is mapped onto an effective Anderson impurity model [13]. This model describes an impurity and its hybridizations with conduction electrons (holes in our case). The mapping onto this model is exact in infinite dimensions [15] and means the restriction to local selfenergy diagrams in finite dimensions.

As first step of our derivation of the cluster/impurity we apply a unitary transformation to the Hamiltonian (2):

$$H = \sum_{\mathbf{k},\sigma} (d_{\mathbf{k}\sigma}^\dagger, p_{\mathbf{k}\sigma}^\dagger, \bar{p}_{\mathbf{k}\sigma}^\dagger) \begin{pmatrix} \varepsilon_d - \mu & -2t\gamma_{\mathbf{k}} & 0 \\ -2t\gamma_{\mathbf{k}} \varepsilon_{p\mathbf{k}} - \mu & t'_{\mathbf{k}} & \\ 0 & t'_{\mathbf{k}} & \varepsilon_{\bar{p}\mathbf{k}} - \mu \end{pmatrix} \begin{pmatrix} d_{\mathbf{k}\sigma} \\ p_{\mathbf{k}\sigma} \\ \bar{p}_{\mathbf{k}\sigma} \end{pmatrix} \quad (4)$$

with

$$\varepsilon_{p\mathbf{k}} = \frac{1}{\gamma_{\mathbf{k}}^2} \{ \sin(\mathbf{k}\mathbf{x})^2 \varepsilon_{p_x} + \sin(\mathbf{k}\mathbf{y})^2 \varepsilon_{p_y} - 8t' \sin(\mathbf{k}\mathbf{x})^2 \sin(\mathbf{k}\mathbf{y})^2 \}, \quad (5)$$

$$\varepsilon_{\bar{p}\mathbf{k}} = \frac{1}{\gamma_{\mathbf{k}}^2} \{ \sin(\mathbf{k}\mathbf{y})^2 \varepsilon_{p_x} + \sin(\mathbf{k}\mathbf{x})^2 \varepsilon_{p_y} + 8t' \sin(\mathbf{k}\mathbf{x})^2 \sin(\mathbf{k}\mathbf{y})^2 \}, \quad (6)$$

$$t'_{\mathbf{k}} = \frac{\sin(\mathbf{k}\mathbf{x}) \sin(\mathbf{k}\mathbf{y})}{\gamma_{\mathbf{k}}^2} \times \{ (\varepsilon_{p_x} - \varepsilon_{p_y}) + 4t' (\sin(\mathbf{k}\mathbf{x})^2 - \sin(\mathbf{k}\mathbf{y})^2) \} \quad (7)$$

and

$$\gamma_{\mathbf{k}}^2 = \sin(\mathbf{k}\mathbf{x})^2 + \sin(\mathbf{k}\mathbf{y})^2. \quad (8)$$

This transformation leads to new orbitals p and \bar{p} . d hybridizes with p but not with \bar{p} . The case of $\varepsilon_{p_x} = \varepsilon_{p_y} = \varepsilon_p$ and $t' = 0$ leads to a dispersionless \bar{p} -band at $\varepsilon_p - \mu$ and the \bar{p} -orbital is decoupled from the rest of the system. This procedure leads to a well-defined description of local orbitals at different lattice cells, which was suggested by Valenti and Gros [14]. Within this formulation the problem how to distribute the p -orbitals, which originally are located in between different Cu -sites, to a particular unit cell was solved. In order to construct a sensible DMFT we here follow a path, which identifies the effective 'impurity' needed to set up the DMFT equations directly from the d -part of the Green's function. Due to the form (4) of the Hamiltonian the general structure for $G_{\mathbf{k}\sigma}^{dd}(z)$ within the DMFT is:

$$G_{\mathbf{k}\sigma}^{dd}(z) = \left[z - \varepsilon_d + \mu - \Sigma_d(z) - \frac{4t^2\gamma_{\mathbf{k}}^2}{z - \varepsilon_{p\mathbf{k}} + \mu - \frac{t_{\mathbf{k}}'^2}{z - \varepsilon_{\bar{p}\mathbf{k}} + \mu}} \right]^{-1}. \quad (9)$$

The sum over \mathbf{k} will in general lead to a complicated structure in the denominator. However, since the selfenergy $\Sigma_d(z)$ is \mathbf{k} -independent we may cast it into the form:

$$G_{\sigma}^{dd}(z) = \frac{1}{N} \sum_{\mathbf{k}} G_{\mathbf{k}\sigma}^{dd}(z) \stackrel{!}{=} \left[z - \varepsilon_d + \mu - \Sigma_d(z) - \frac{t_0^2}{z - \varepsilon_{p00} + \mu - \Delta(z)} \right]^{-1}, \quad (10)$$

where t_0 and ε_{p00} are Fourier-transformed terms of $-2t\gamma_{\mathbf{k}}$ and $\varepsilon_{p\mathbf{k}}$. The effective medium's function $\Delta(z)$ is defined through equation (10) and incorporates all bandstructure effects due to the dispersion and hybridizations. Note that this definition is far from being unique! In fact we may choose for example

$$\frac{1}{N} \sum_{\mathbf{k}} G_{\mathbf{k}\sigma}^{dd}(z) \stackrel{!}{=} [z - \varepsilon_d + \mu - \Sigma_d(z) - \tilde{\Delta}(z)]^{-1} \quad (11)$$

as another possibility. In this case the equation defining the DMFT would be formally the same as for the one-band Hubbard model. However, due to the singular structure induced by a d - p -hopping equation (10) turns out to be numerically more convenient: For $\Delta(z) = 0$ the level structure of the d - p complex is already included from the outset and $\Delta(z)$ is rather smooth. On the other hand the at the first glance more natural choice (11) would result in a $\tilde{\Delta}(z)$ with a highly singular behaviour reflecting the existence of unrenormalized p -states. Thus the Hamiltonian

of the effective impurity is defined by:

$$H = \sum_{\sigma} (\varepsilon_d - \mu) d_{\sigma}^{\dagger} d_{\sigma} + \sum_{\sigma} (\varepsilon_{p00} - \mu) p_{\sigma}^{\dagger} p_{\sigma} + \sum_{\sigma} (t_0 d_{\sigma}^{\dagger} p_{\sigma} + h.c.) + U_d d_{\uparrow}^{\dagger} d_{\downarrow}^{\dagger} d_{\downarrow} + \sum_{\mathbf{k},\sigma} (V_{\mathbf{k}} p_{\sigma}^{\dagger} c_{\mathbf{k},\sigma} + h.c.) + \sum_{\mathbf{k},\sigma} \varepsilon_{\mathbf{k}} c_{\mathbf{k},\sigma}^{\dagger} c_{\mathbf{k},\sigma}, \quad (12)$$

with a hybridization $V_{\mathbf{k}}$ of the p -orbitals to the effective medium described by the dispersion $\varepsilon_{\mathbf{k}}$. The effective medium enters the solution of the impurity problem only by the hybridization function

$$\Delta(z) = \frac{1}{N} \sum_{\mathbf{k}} \frac{|V_{\mathbf{k}}|^2}{z - \varepsilon_{\mathbf{k}}}. \quad (13)$$

of the p -states, which has to be determined selfconsistently from equation (10).

Thus equation (10) is the central point of our selfconsistency scheme. After calculating the local Green's function by the sum of \mathbf{k} one can extract the hybridization function $\Delta(z)$, which is used to solve the impurity problem with help of an extended NCA scheme [8]. From the impurity Green's function for the d -orbital we extract the selfenergy $\Sigma(z)$, which is then used in the calculation of the lattice Green's function in equation (10).

3 The effective two-band model

Let us begin the discussion of the properties of the three-band Hubbard model by considering the standard case $\varepsilon_p = \varepsilon_{p_x} = \varepsilon_{p_y}$ and $t' = 0$. Then the non-hybridizing \bar{p} -orbital decouples from the rest of the system leading to a two-band problem. This problem can in principle be generalized to D dimensions, but it is impossible to find a uniform scaling to obtain a nontrivial limit $D \rightarrow \infty$ [14]. The DMFT used here therefore always leads to an approximate treatment of the model. In order to simplify numerical calculations the semi-elliptic density of states is used, i.e.:

$$G_d(z) = \frac{1}{N} \sum_{\mathbf{k}} \frac{1}{z - (\varepsilon_d - \mu) - \Sigma(z) - \frac{4t^2\gamma_{\mathbf{k}}^2}{z - (\varepsilon_p - \mu)}} = \int d\varepsilon \frac{\rho_o(\varepsilon)}{z - (\varepsilon_d - \mu) - \Sigma(z) - \frac{4t^2(1 - \varepsilon)}{z - (\varepsilon_p - \mu)}}, \quad (14)$$

with $\rho_o(\varepsilon) = \frac{2}{\pi} \sqrt{1 - \varepsilon^2}$. The Green's function for the p -orbital is obtained, if one exchanges the energies $\varepsilon_d + \Sigma(z)$ and ε_p .

3.1 One-particle spectra

Figures 2a and 2b show the one-particle spectra for the d -orbital and the hybridizing p -orbital for an electron and a hole doped system, respectively, at room temperature, i.e. at a reciprocal temperature of $\beta = 40 \text{ eV}^{-1}$. They show in terms of the hole picture from the left to the right: the lower Hubbard band, the Zhang-Rice band mostly due to excitations into a two particle singlet state, the p -band and the upper Hubbard band, which has a double peak structure due to the complex excitation capabilities of the cluster under consideration. In both figures typical particle hole excitations are marked by arrows, which play a role in the dynamical conductivity (see section 3.2). In addition to those expected structures a sharp resonance appears near the Fermi energy in both doping regimes. From the DMFT of the one-band Hubbard model it is well known [16], that this resonance is connected to a local Kondo-like screening. It thus is frequently termed Abrikosov-Suhl resonance to stress the similarity of its physics to the Kondo effect. For a detailed description of the doping and temperature dependencies of the spectral weights see ref. [8].

3.2 The in-plane conductivity

In order to calculate the in-plane conductivity in linear response theory using Kubo's formula, one has to derive the current-current correlation function. The current density operator for the three-band model (see equation (1)) is given by the time derivative of the polarization operator using Heisenberg's equation of motion. This procedure leads to the expression:

$$\mathbf{j} = -\frac{2et}{\hbar} \sum_{\nu} \sum_{\mathbf{k}, \sigma} \mathbf{r}_{\nu} \sin(\mathbf{k}\mathbf{r}_{\nu}) (d_{\mathbf{k}, \sigma}^{\dagger} p_{\nu \mathbf{k}, \sigma} + p_{\nu \mathbf{k}, \sigma}^{\dagger} d_{\mathbf{k}, \sigma}),$$

with the vector \mathbf{r}_{ν} connecting d - and p -sites.

In the following the real part of the in-plane conductivity in x-direction is examined. The current-current correlation function is calculated within the orbital representation of equation (4). Since the particle-hole excitations with the non-hybridizing \bar{p} -states are playing a role only at high energies, contributions with \bar{p} -orbitals are neglected. Thus we obtain:

$$\begin{aligned} \Re \{\sigma_x(\omega)\} &= \frac{1}{2} (\Re \{\sigma_x(\omega)\} + \Re \{\sigma_y(\omega)\}) = \\ &= \frac{1}{2} \left(\frac{aet}{\hbar}\right)^2 \frac{1}{N} \sum_{\mathbf{k}} \frac{\sin(\mathbf{k}\mathbf{r}_x)^4 + \sin(\mathbf{k}\mathbf{r}_y)^4}{\gamma_{\mathbf{k}}^2} \times \\ &\quad \int_{-\infty}^{\infty} d\varepsilon \frac{f(\varepsilon) - f(\varepsilon + \omega)}{\omega} \Pi(\varepsilon, \omega, \mathbf{k}) \end{aligned}$$

with

$$\Pi(\varepsilon, \omega, \mathbf{k}) = \sum_{(\alpha, \beta)} \rho_{\alpha}(\varepsilon + \omega, \mathbf{k}) \rho_{\beta}(\varepsilon, \mathbf{k})$$

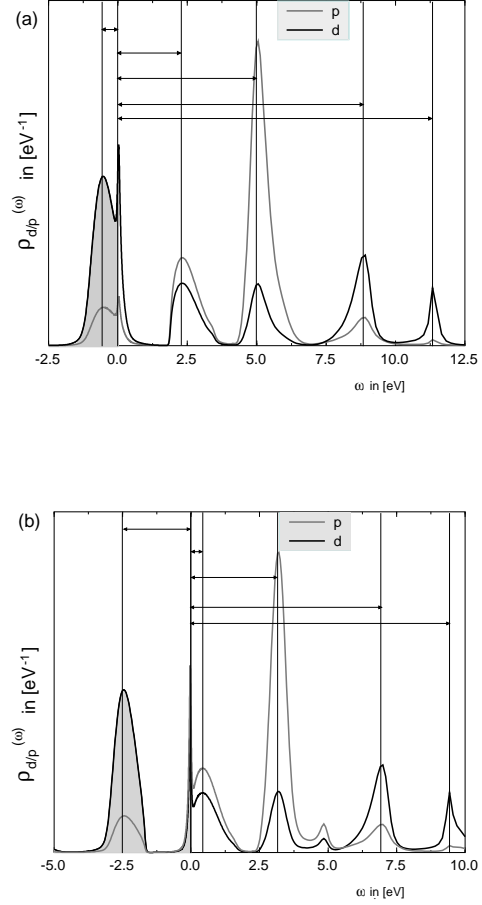


Fig. 2. One-particle spectra for the d -orbital and the hybridizing p -orbital in a electron doped system (a) and in a hole doped system (b) for energies in units of the hopping parameter t . The parameter set was $\beta = 40.0 \text{ eV}^{-1}$, $\Delta = 3.6 \text{ eV}$, $t = 1.0 \text{ eV}$ and $U_d = 7.2 \text{ eV}$.

and spectral function ρ_{α} of Green's functions with the following orbital combinations:

$$(\alpha, \beta) \in \{(pp^{\dagger}, dd^{\dagger}), (dd^{\dagger}, pp^{\dagger}), (pd^{\dagger}, pd^{\dagger}), (dp^{\dagger}, dp^{\dagger})\}.$$

Due to the locality of the vertex kernel and the antisymmetric current operator vertex corrections vanish analogously to calculations for the one-band Hubbard model [17]. Finally the \mathbf{k} -summation is carried out in an averaged way by integration over the pure density of states:

$$\begin{aligned} \Re \{\sigma(\omega)\} &= \\ &= \sigma_o \int_{-\infty}^{\infty} \int_{-\infty}^{\infty} d\varepsilon d\tilde{\varepsilon} \rho_o(\tilde{\varepsilon}) \frac{f(\varepsilon) - f(\varepsilon + \omega)}{\omega} \Pi(\varepsilon, \omega, \tilde{\varepsilon}). \end{aligned}$$

Typical particle-hole excitations for electron and hole doped systems are denoted by the vertical arrows in figure 2a and 2b. These different excitations can in principle all be resolved in the graph of the conductivity. However, for sake of simplicity only the low energy scale is shown in figures 3a and 3b. The in-plane conductivity was cal-

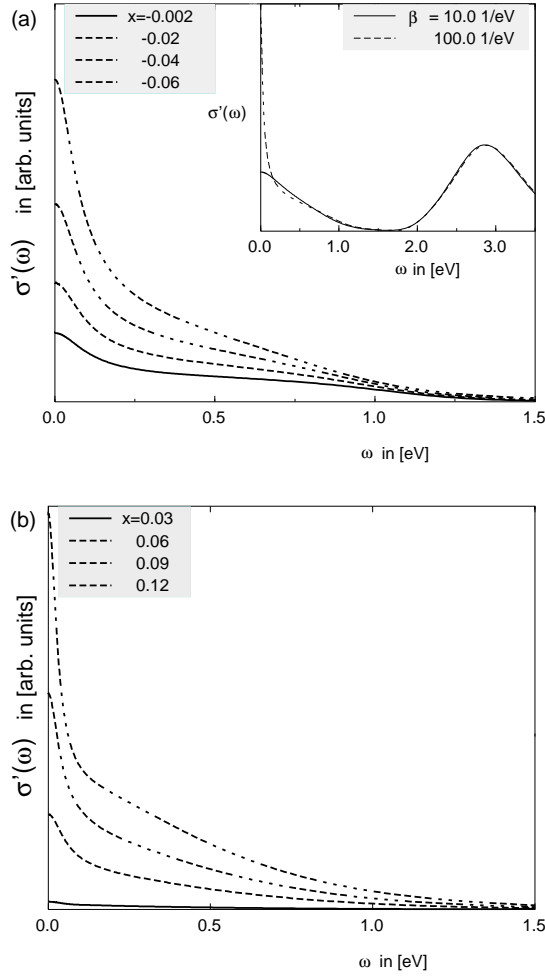


Fig. 3. Real part of the conductivity for several electron doped (a) and several hole doped systems (b) at $\beta = 40 \text{ eV}^{-1}$. The inset shows the temperature dependency for a system with the doping level $x = -4\%$.

culated for several doping parameters x for a reciprocal temperature $\beta = 40 \text{ eV}^{-1}$. The temperature dependency for constant doping x is shown in the inset of the figure 3a. Both electron and hole doped systems show an increasing conductivity upon doping in the mid-infrared region at 0.5 eV . The far-infrared part of the conductivity shows a pronounced increase due to the growth of spectral weight of the Abrikosov-Suhl resonance upon doping. In the inset of figure 3a the strong temperature dependency of the low energy excitations is shown. The broad peak at 3 eV shown in the inset corresponds to transitions between the lower Hubbard band and the Zhang-Rice band. The energy separation of these two bands, which describes the optic energy gap Δ_{opt} , is smaller than the bare charge transfer energy $\Delta = \varepsilon_p - \varepsilon_d$. For example, for the present set of parameters we find $\Delta_{opt} \approx 2 \text{ eV}$, which is in good agreement with measurements by Uchida et al. [18] for $\text{La}_{2-x}\text{Sr}_x\text{CuO}_4$ and $\text{Nd}_{2-x}\text{Ce}_x\text{CuO}_{4-y}$.

4 Results for a quadratic CuO_2 -system

In this section we present results for a two-dimensional tight-binding model. At a first glance the use of the DMFT as an approximation may seem to be particularly crude. However, as long as the system is not too close to a phase transition the choice of a local selfenergy appears to capture the most important dynamics, which is seen if one compares the results from a local approximation with those of a Monte Carlo calculation in the two dimensional one-band Hubbard model [19].

4.1 Bandstructure and Fermi surface

Before we discuss the bandstructure for the correlated electron system, let us look at the uncorrelated tight-binding bandstructure, which is shown in figure 4. In the following the name of the bands is given by their main orbital character. Here the band with the lowest energy (hole picture) has primarily d -character. The upper bands have p -character. For hole-doping the Fermi energy lies in the upper bands, for electron-doping in the lower band. The d -band has a minimum at the M -point and a saddle point at the X -point. With increasing value of t'/t the distance between the minimum and the saddle point increases. This means that the region of electron doping, where one can find a Fermi surface surrounding the M -point by adjusting the chemical potential μ , is also increasing. In the hole doped case, however, a positive value of t'/t leads to a Fermi surface centered around Γ produced by the hybridizing p -band and one around M by the non-hybridizing \bar{p} -band, since the non-hybridizing p -band is pushed towards the hybridizing p -band with an increasing value of t'/t . On the other hand, a value $t'/t < 0$

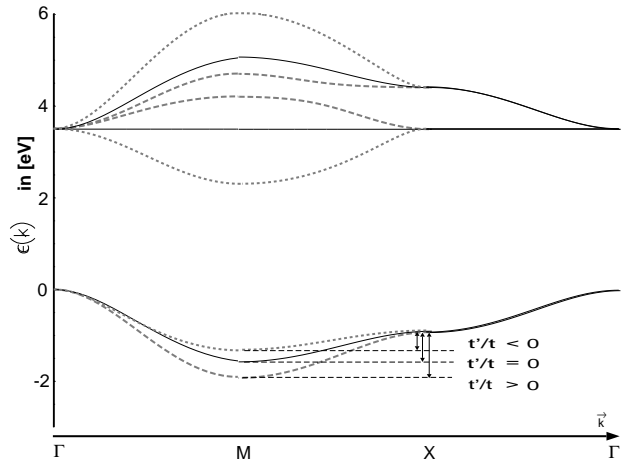


Fig. 4. Tight-binding bandstructure for several values of t'/t . $\varepsilon_d = 0 \text{ eV}$, $\varepsilon_p = 3.6 \text{ eV}$, $t = 1 \text{ eV}$ and $t' = 0, \pm 0.3 \text{ eV}$.

would push down the non-hybridizing \bar{p} -band, leading to a dispersion minimum at the M -point, as it is observed experimentally [20]. Thus the requirement of a Fermi surface surrounding the M -point for both electron and hole

doping means that one either has to assume different signs for t' in the two cases of doping or look for a more subtle mechanism leading to the observed physics for a fixed sign of t' .

In the following we want to argue that in order to solve the puzzle of the correct choice of the parameter t' , one has to consider electronic correlations. In order to make contact with the free bandstructure we plot the total spectral weight $A(\mathbf{k}, \omega)$ in a density-plot in the ω - \mathbf{k} -plane. The dark regions refer to high spectral weight. In figure 5a and 5b the low energy part of the resulting \mathbf{k} -dependent total spectral weight for the electron and hole doped CuO_2 -plane is shown. These plots show the lower Hubbard band, the Abrikosov-Suhl resonance and the Zhang-Rice band. These bands exhibit the typical dispersion of the tight-binding d -band. On the other hand the p -bands and the

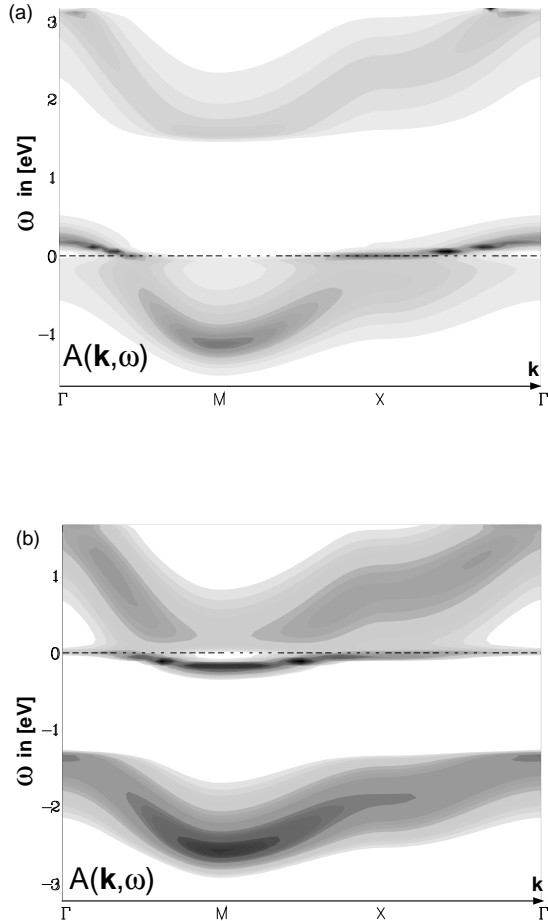


Fig. 5. Total spectral weight in a density-plot in the ω - \mathbf{k} -plane for special \mathbf{k} -points for $\beta = 40 \text{ eV}^{-1}$, $t = 1 \text{ eV}$, $t' = 0.3 \text{ eV}$, $\Delta = 3.6 \text{ eV}$, $U_d = 7.2 \text{ eV}$ and $x = -8.5\%$ (a), $x = +8.5\%$ (b).

upper Hubbard band at higher energies (not shown in the figure) have the dispersion of their uncorrelated pendants. For both types of doping there occurs a quasi-particle Abrikosov-Suhl resonance at the Fermi energy. It is important to note, that the dispersion of this band (which has d -character) completely determines the shape of the Fermi

surface. In figure 6 we show, that for constant doping pa-

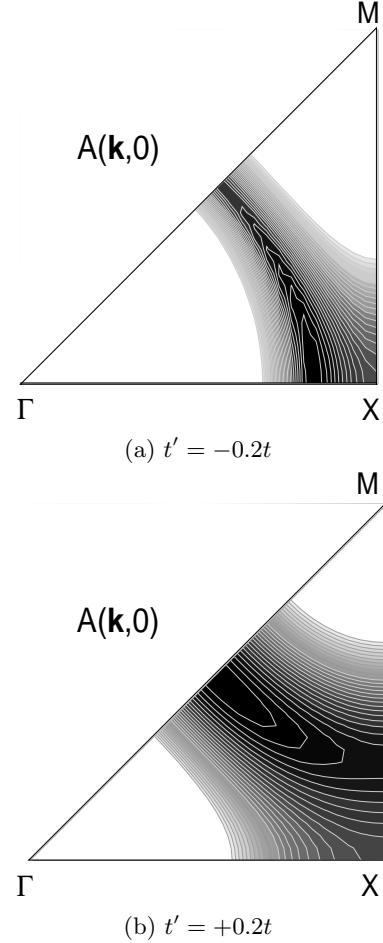


Fig. 6. Total spectral weight at the Fermi energy in a density-plot for two values of t'/t in the irreducible part of the Brillouin zone. The doping is $x = +5\%$ in both cases, the remaining parameters are the same as in figure 5. One can see that the choice of t'/t determines the shape of the Fermi surface.

rameter $x = +5\%$, one can change the shape of the Fermi surface by varying the value of t'/t , since it directly influences the dispersion of the band. From the experimental fact that the Fermi surface encloses the M -point we are led to a value $t'/t > 0$, which is in agreement with those anticipated for high- T_c compounds such as $\text{Nd}_{2-x}\text{CeCuO}_4$ [21] or $\text{Bi}_2\text{Sr}_2\text{CaCu}_2\text{O}_{8+x}$ [22].

4.2 Electronic Response to a frozen phonon excitation

In this section we investigate the response of the oxygen occupation on a level splitting of the p_x - and p_y -states. Such a level splitting may be realized by a different displacement in z -direction of the x - and y -oxygen in the CuO_2 -plane. For simplicity we treat a symmetric energy-level splitting, i.e. one has to modify equation (7) to (9) with $\varepsilon_{p_x/y} = \varepsilon_p \pm \delta\varepsilon_p$. With this modification we can look

at the static density-density correlation function in linear response approximation:

$$\langle\langle\delta\hat{n}_{xy},\delta\hat{n}_{xy}\rangle\rangle_{(\omega=0)}\equiv\frac{\delta\langle\hat{n}_x\rangle-\delta\langle\hat{n}_y\rangle}{\delta\varepsilon_p}\quad(15)$$

This quantity can be used to examine the electron-phonon coupling for the B_{1g} -phonon in high- T_c -compounds. Of course it is not possible to study the dynamical aspects of the coupling, but it is a rough measure for the renormalization of the phonon-frequency due to this coupling.

Up to $\delta\varepsilon_p = 0.075$ eV the correlation function was found to be independent on $\delta\varepsilon_p$ for all considered sets of parameters. The static susceptibility was therefore investigated for a constant value of the level splitting, $\delta\varepsilon_p = 0.05$ eV. In figure 7 we show the density-density correlation for $t'/t = 0.5$ for several temperatures as a function of the doping x . The dashed line marks the doping which

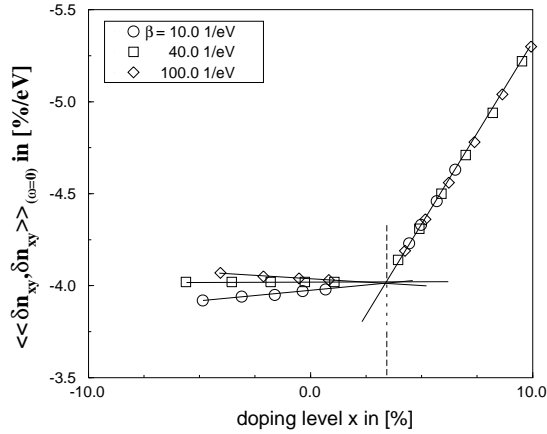


Fig. 7. Static density-density correlation at three different reciprocal temperatures β for $\delta\varepsilon_p = 0.1$ eV, $t'/t = 0.5$, $U_d = 7.2$ eV and $\Delta = 3.6$ eV.

is found, when the chemical potential μ is in the gap. Note that the crossing point is not exactly at $x = 0$. Thus the doping x cannot be identified with the doping level of a real CuO_2 -plane. This shortcoming originates from a numerical failure of the NCA and is enhanced by a large value of $t'/t = 0.5$. This effect can be neglected in the previous section 3, where for $t' = 0$ the model doping level x for the insulating case was less than 1%. For clarity we term the region left to the dashed line in figure 7 as electron doping and the one right as hole doping. In both regimes the density response is a linear function of the doping x . This holds for all investigated sets of parameters. In the hole doped regime the density-density correlation shows in addition no effect upon changing the temperature and it can be described by a straight line with a slope $\partial\langle\langle\delta\hat{n}_{xy},\delta\hat{n}_{xy}\rangle\rangle_{(\omega=0)}/\partial x \approx -6$ eV $^{-1}$. For electron doped systems the slope increases with decreasing temperature. In figure 8 the hole-density response of p -orbitals is shown together with occupation of p - and d -states for different doping. It can be seen that the density response is strong in the hole doped regime ($x > 3\%$), when also the number of holes in the p -states is large.

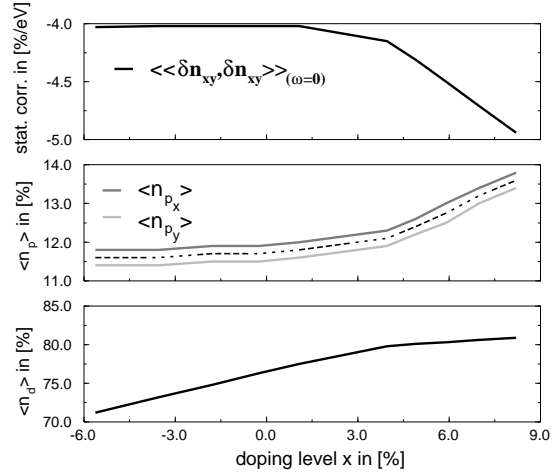


Fig. 8. Comparison of the static density-density correlation with the occupancies of the different orbitals for $\delta\varepsilon_p = 0.1$ eV, $t'/t = 0.5$, $U_d = 7.2$ eV, $\Delta = 3.6$ eV and $\beta = 40$ eV $^{-1}$.

We have also calculated the hole-density response function for d -states at (π, π) . This function is rather independent of the Coulomb parameter U_d , but depends on the occupancy of the d -orbitals. For a calculation with $t' = 0$ the strength of the d -response varies by a factor 3 to 4 compared to the p -response due to the larger number of occupied d -orbitals.

5 Summary

In this paper we presented results for the electronic properties of the three-band Hubbard model obtained with the help of the Dynamical Mean-Field Theory. For the calculations we used two different model density of states: a simple elliptic density of states to calculate the local spectral density and the optical conductivity, a two dimensional tight-binding density to calculate the details of the bandstructure and a static response function.

The spectral density consists of a lower Hubbard band with d -character, transitions into a Zhang-Rice band of p - d -singlet states, binding and non-binding p -bands, and an upper Hubbard band. For electron doping the Fermi level is in the lower Hubbard band, for hole doping in the Zhang-Rice band. The energy separation between these two bands, which is the optical gap Δ_{opt} typically seen in conductivity measurements, is smaller than the bare energy separation of p - and d -states, $\Delta = \varepsilon_p - \varepsilon_d$. This tendency as well as the calculated value of Δ_{opt} qualitatively agree with experimental observed data.

At low energies the optical conductivity shows a narrow Drude-like peak on a broad background as experimentally observed. The narrow Drude peak is due to transitions inside the Kondo-like feature close to the Fermi energy.

We studied in detail the influence of an additional tight-binding coupling t' between oxygen states on the bandstructure. It turned out that in the presence of correlations the variation of the Fermi surface is consider-

ably changed compared to the non-interacting system. The most important aspect is that one finds similar structures of the Fermi surface for both electron and hole doped systems. Together with the experimental fact that the Fermi surface encloses the M -point for both kind of doped systems we conclude that t'/t must be positive.

We also investigated the response of the occupation-difference of p -states on the energy splitting of the two different p -states in the unit cell. Such a response function is a measure for the electron-phonon coupling of special phonons. Naturally this density response increases with the occupation number of p -holes, i.e. it is larger if the Fermi energy is in the Zhang-Rice band than in the lower Hubbard band.

Acknowledgements: This work was partially supported by the DFG grant PR 289/5.

References

1. J. G. Bednorz, K. A. Müller, Z.Phys. B **64**, (1986) 189.
2. E. Dagotto, Rev.Mod.Phys. **66**, (1994) 763.
3. J. Hubbard, Proc.Roy.Soc. A **276**, (1963) 238; J. Kanamori, Prog. Theor. Phys,**30**,(1963) 275; M. C. Gutzwiller, Phys. Rev. Lett. **10**,(1963) 59.
4. N. F. Mott, *Metal-Insulator Transitions*, 2nd ed., (Taylor and Francis, London, 1990).
5. C. Almasan, M. B. Maple, *Chemistry of High-Temperature Superconductors* (ed. C. M. Rao, World Scientific, Singapore, 1991).
6. P. Fulde, *Electron Correlation in Molecules and Solids* (Springer-Verlag, Berlin Heidelberg, 1995) 14.2 .
7. V. Emery, Phys.Rev.Lett. **58**, (1987) 2794.
8. J. Schmalian, P. Lombardo, M. Avignon, K. H. Benneman, Physica B **223-224**, (1996) 602; P. Lombardo, M. Avignon, J. Schmalian, K. H. Benneman, Phys.Rev. B **54**, (1996) 5317.
9. H. Watanabe, S. Doniach, Phys.Rev. B **57**, (1998) 3829.
10. Th. Maier, M. Zöfl, Th. Pruschke, J. Keller, to be published.
11. J. Zaanen, G. A. Sawatzky, J. W. Allen, Phys.Rev.Lett. **55**, (1985) 418.
12. M. S. Hybertsen et al., Phys.Rev. B **41**, (1990) 11068.
13. P. W. Anderson, Phys.Rev. **124**, (1961) 41
14. R. Valenti, C. Gros, Z. Phys. B **90**, (1993) 161.
15. W. Metzner, D. Vollhardt: Phys. Rev. Lett. **62**,(1989) 324.
16. Th. Pruschke, Adv. in Phys. **44**, (1995) 187; A. Georges, G. Kotliar W. Krauth, M. J. Rozenberg, Rev. of Mod. Phys. **68**, (1996) 13.
17. Th. Pruschke, D. L. Cox, M. Jarrell, Phys.Rev. B **47**, (1993) 3553.
18. S. Uchida et al., Phys.Rev. B **43**, (1991) 7942.
19. Th. Pruschke, Th. Obermeier, J. Keller, M. Jarrell, Physica B **223,224**, (1996) 611.
20. Z. X. Shen, D. S. Dessau, Phys. Rep. **253**, (1995) 1-162.
21. D. M. King et al., Phys.Rev.Lett. **70**, (1993) 3159.
22. D. S. Dessau et al., Phys.Rev.Lett. **71**, (1993) 2781.